










RESEARCH ARTICLE | NOVEMBER 21 2024

Meta-optics triplet for zoom imaging at mid-wave infrared



Special Collection: [Mid and Long Wavelength Infrared Photonics, Materials, and Devices](#)

Anna Wirth-Singh   ; Arturo Martin Jimenez  ; Minhoo Choi  ; Johannes E. Fröch  ; Rose Johnson  ; Tina Le Teichmann; Zachary Coppens  ; Arka Majumdar  

 Check for updates

Appl. Phys. Lett. 125, 211705 (2024)

<https://doi.org/10.1063/5.0227368>



Articles You May Be Interested In

Experimental demonstration of a continuous varifocal metalens with large zoom range and high imaging resolution

Appl. Phys. Lett. (October 2019)

Practical error estimation in zoom-in and truncated tomography reconstructions

Rev. Sci. Instrum. (June 2007)

A novel smooth impact drive mechanism actuation method with dual-slider for a compact zoom lens system

Rev. Sci. Instrum. (August 2011)

25 November 2024 21:44:20



Applied Physics Letters

Special Topics Open for Submissions

[Learn More](#)



Meta-optics triplet for zoom imaging at mid-wave infrared

Cite as: Appl. Phys. Lett. **125**, 211705 (2024); doi: [10.1063/5.0227368](https://doi.org/10.1063/5.0227368)

Submitted: 8 July 2024 · Accepted: 31 October 2024 ·

Published Online: 21 November 2024



View Online



Export Citation



CrossMark

Anna Wirth-Singh,^{1,a)}  Arturo Martin Jimenez,²  Minhho Choi,³  Johannes E. Fröch,^{1,3}  Rose Johnson,³ 
Tina Le Teichmann,¹ Zachary Coppens,²  and Arka Majumdar,^{1,3,a)} 

AFFILIATIONS

¹Department of Physics, University of Washington, Seattle, Washington 98195, USA

²CFD Research Corporation, 6820 Moquin Dr. NW, Huntsville, Alabama 35806, USA

³Department of Electrical and Computer Engineering, University of Washington, Seattle, Washington 98195, USA

Note: This paper is part of the APL Special Collection on Mid and Long Wavelength Infrared Photonics, Materials, and Devices.

a) Authors to whom correspondence should be addressed: arka@uw.edu and annaw77@uw.edu

ABSTRACT

Lenses with dynamic focal length, also called zoom functionality, enable a variety of applications related to imaging and sensing. The traditional approach of stacking refractive lenses to achieve this functionality results in an expensive, heavy optical system. Especially for applications in the mid-infrared, light weight and compact form factor are required. In this work, we use a meta-optic triplet to demonstrate zoom imaging at mid-wave infrared wavelengths. By varying the axial distances between the optics, the meta-optic triplet achieves high-quality imaging over a zoom range of $5\times$, with a 50° full field of view in the widest configuration and an aperture of 8 mm. This triplet system demonstrates the potential for meta-optics to reduce conventional components in complex and multi-functional imaging systems to dramatically thinner and lighter components.

Published under an exclusive license by AIP Publishing. <https://doi.org/10.1063/5.0227368>

Thermal imaging has extensive applications in defense, night vision, and meteorology.^{1–4} In particular, the mid-wave infrared (MWIR, $3\text{--}5\ \mu\text{m}$) is especially attractive for long-range imaging and sensing due to its superior penetration in high-humidity atmospheric conditions.⁵ Wide field of view and high resolution are often desirable for these imaging applications. For imaging dynamic targets, it is particularly helpful to have both wide field of view images for context and narrow field of view for zoomed-in detail, with rapid switching mechanism between the views. However, achieving both qualities simultaneously requires a large, high-resolution camera sensor, and such sensors are particularly expensive at MWIR wavelengths. Alternatively, these applications can benefit from zoom functionality, wherein the image magnification is changed by repositioning optics within the lens system so that a range of image magnifications can be captured using a single aperture and sensor.

Most conventional zoom systems are composed of a series of refractive lenses, some of which are axially translated to change the zoom state. While effective, stacked refractive lenses quickly become heavy, which is undesirable for many applications where zoom functionality is required, such as airborne scopes and cameras. Due to the long total track length of zoom imaging systems, excess weight can

cause significant torque on the mechanical support system. In addition, to achieve high-quality imaging with zoom constraints, aspheric lenses are often used^{1,6} that are difficult to manufacture due to non-constant curvature across the surface. Combined with the limited availability of suitable materials for MWIR refractive lenses, such as germanium and calcium fluoride, this contributes to the increased cost of thermal zoom imaging systems.

Ultra-thin meta-optics have demonstrated great potential to miniaturize imaging systems, including those at MWIR wavelengths.^{7–11} However, introducing zoom functionality into meta-optics, and other forms of metasurfaces, is challenging. Various techniques have been employed, including mechanical stretching,^{12–14} MEMS,¹⁵ liquid crystals,^{16,17} and Alvarez^{18,19} lenses, but these techniques are limited in zoom range and aperture. Similarly to the conventional approach of stacking a series of refractive lenses, meta-optics can also be stacked to improve imaging performance. Meta-optic doublets for applications including aberration correction^{20,21} and large field of view²² have been demonstrated, but without a tuning mechanism. Recently, researchers have demonstrated zoom imaging by axial translation in a doublet lens system at 940 nm using two meta-optics with extended depth of focus for extended zoom range, but for a relatively small aperture of 1 mm.⁶

Further extension into triplet meta-optic systems is a relatively unexplored area, with existing demonstrations focused mainly on chromatic aberration correction.^{23,24}

In this work, we demonstrate an 8 mm aperture, 50° full field of view (FoV) zoom imaging meta-optic triplet at 3.4 μm wavelength. We follow the traditional approach by varying the position of two of the three meta-optic elements, while keeping the meta-optic phase profiles fixed, to increase the image magnification from 1× to 5×. Additionally, our zoom imaging system is parfocal, meaning that the focal plane remains fixed while achieving the intermediate zoom states. For optimal transmission through the triplet lens system, we realize the meta-optics in a silicon-on-sapphire material platform. We demonstrate high-quality imaging performance up to 50° FoV in the wide field of view configuration. This development enables MWIR applications with zoom functionality and lightweight multi-element imaging systems.

The design of the meta-optic zoom lens follows a standard three-element zoom structure. In order to keep a fixed back focal length, a mechanically adjustable afocal frontend determines the size of the beam on the back imaging lens, which remains a fixed focal length from the sensor.² The zoom behavior of the designed system is schematically depicted in Fig. 1. The system is optimized for five discrete zoom states, denoted configurations 1 through 5, with this change accomplished by varying the axial distances between the metasurfaces

while the phase profiles of the meta-optics themselves remain fixed. Specifically, the meta-optic nearest the sensor, termed the focusing optic, remains a fixed 15 mm distance from the sensor while the positions of the other two optics (denoted as the compensator optic nearest the object and the variator optic in the middle) are adjusted to change the zoom state. This change is primarily accomplished by axially translating the variator optic, which is adjusted within a range of 14.6 mm. The compensator optic has negative power to defocus the light and its axial position is adjusted within a smaller range of 5.21 mm to correct for aberrations. Ray tracing diagrams of all configurations are shown in Fig. 1(a). The process by which the optimized phase profiles were obtained is described in greater detail below.

The phase profiles of the meta-optics were optimized using commercial ray tracing software (Zemax OpticStudio). Each meta-optic was modeled as a Binary-2 phase profile according to the following equation:

$$\Phi(\rho) = \sum_{i=1}^6 A_i \left(\frac{\rho}{M}\right)^{2i}, \quad (1)$$

where M is a normalization constant, ρ is the radial coordinate, and A_i are polynomial coefficients. To optimize the zoom system, we initially varied the phase profile coefficients A_i and fixed them to optimize

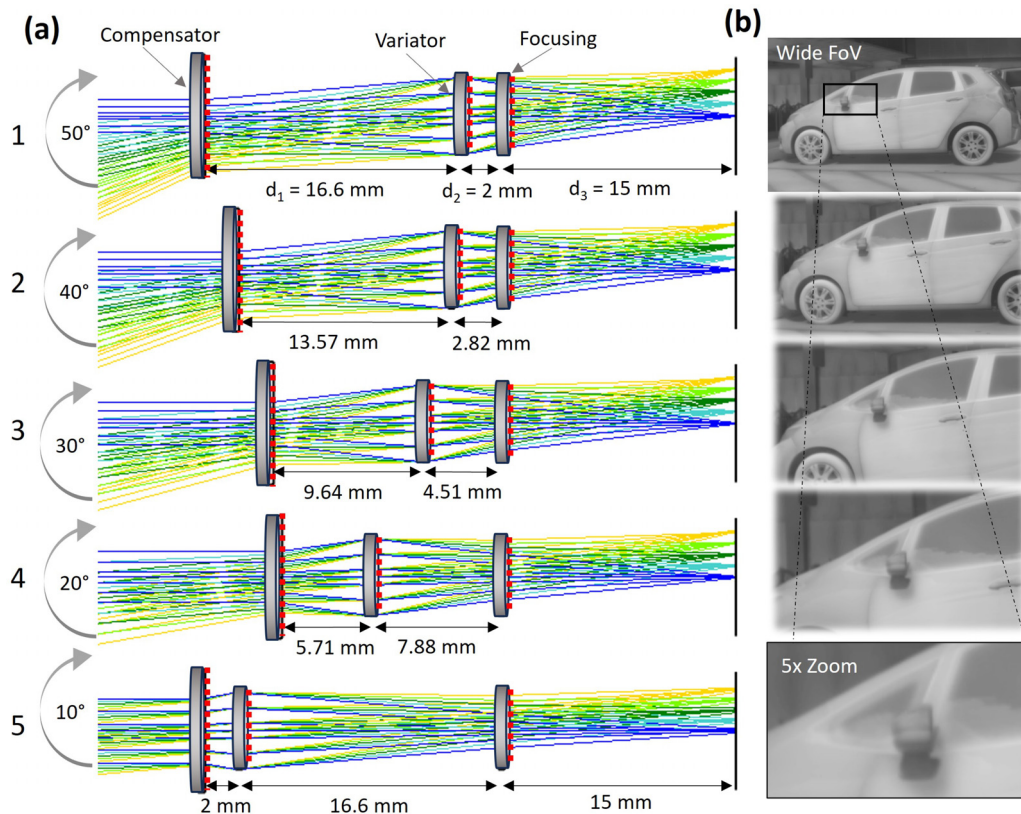


FIG. 1. The zoom lens concept. (a) Ray tracing diagrams for all five configurations. By translating the compensator and variator optics, the effective focal length of the system is changed from a wide field of view (top) to a narrow field of view (bottom). The blue lines represent normally incident rays, while the yellow rays represent 25° and 5° angle of incidence for the wide and narrow configurations, respectively. Intermediate angles are shown in shades of green. (b) Schematic depiction of zoom imaging on an image of a car taken with a thermal camera. As the magnification is increased, the field of view decreases, but the details of the side mirror and windows become clear.

TABLE I. System design specifications.

Configuration	1 (wide)	2	3 (mid)	4	5 (tele)
F Number	3.71	3.94	4.40	5.33	7.98
EFL (mm)	8.78	10.53	14.19	21.74	43.89
Full FoV	50°	40°	30°	20°	10°
d_1 (mm)	16.60	13.57	9.64	5.71	2.00
d_2 (mm)	2.00	2.82	4.51	7.88	16.60

performance at both the tele and wide configurations at predetermined positions. Specifically, wavefront error (with respect to an ideal spherical wavefront) was defined as the merit function during optimization. The optimized coefficients of each metasurface are provided in the [supplementary material](#). Once the phase for each metasurface was determined, the spacings between the surfaces were varied to optimize performance at the intermediate zoom states. As labeled in [Fig. 1\(a\)](#), the distance between the compensator and variator optics is denoted d_1 and the distance between the variator and the focusing optics is denoted d_2 . The distance between the focusing lens and the image plane, denoted d_3 , was held constant at 15 mm while d_1 and d_2 were allowed to vary.

The designed F-number, effective focal length (EFL), and full field of view of each configuration are summarized in [Table I](#). Configuration 1, also called the “wide” configuration, provides the widest field of view at 50° full FoV and F-number of 3.7. Configuration 5, also called the “tele” configuration, provides the most zoomed-in image with 10° full FoV at an F-number of 8.0. The intermediate configurations 2–4 provide equally spaced intermediate zoom states.

The meta-optics are physically realized as crystalline silicon pillars on sapphire substrate (commercially available from UniversityWafer).

While silicon is transparent at MWIR wavelengths, bulk silicon incurs significant Fresnel reflections due to its high index of refraction ($n=3.5$) as compared to the air ($n=1$).²⁵ Therefore, to provide increased transmission efficiency in the multi-layer system, we chose sapphire ($n=1.7$) substrate. Transmission through the sapphire substrate is expected to be 93%. The silicon pillars are 1.5 μm tall arranged on a lattice with periodicity 1.5 μm , and the sapphire substrate thickness is 460 μm . Using rigorous coupled wave analysis,²⁶ we simulated the phase and transmission of silicon pillars as a function of pillar width as shown in [Fig. 2\(c\)](#). From these results, we selected ten pillars with widths ranging from 500 nm to 1.0 μm to comprise the pillar library.

The meta-optics were fabricated using electron beam lithography and inductively coupled plasma etching. All three meta-optics were fabricated from a single 1.5 μm thick silicon-on-sapphire wafer that was diced into chips. Each sample was cleaned in acetone and isopropyl alcohol before an oxygen plasma treatment to promote resist adhesion. Next, we spin-coated ZEP-520A resist and exposed the resist by electron beam lithography. After writing the pattern, we developed the resist in amyl acetate followed by a short oxygen plasma treatment to remove residue. In order to achieve a large etching depth of 1.5 μm , we deposited a hard mask for etching. Specifically, we deposited 70 nm of alumina on top of the patterned samples via electron beam evaporation. To form the hard mask, we lift-off the resist with N-Methyl-2-pyrrolidone. Finally, the silicon was etched via reactive ion etching with SF₆ and C₄F₈ gas chemistry.

Top-down and oblique scanning electron microscope (SEM) images of the fabricated optics are shown in [Figs. 2\(a\)](#) and [2\(b\)](#), respectively, illustrating the fabrication quality. A photograph of the fabricated optics is shown in [Fig. 2\(d\)](#). Except for the meta-optic area, the thin silicon layer has been etched away, revealing the transparent substrate. The surface of the optic, while appearing opaque brown under visible illumination, is transparent under infrared illumination.

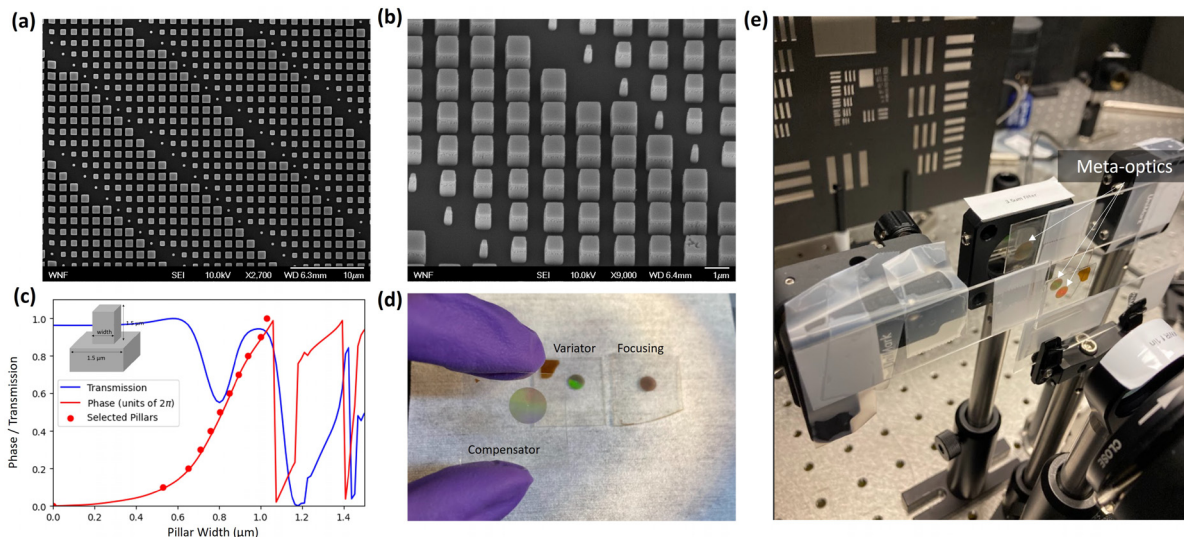


FIG. 2. Metasurface design and fabrication. (a) Top-down SEM image of a fabricated optic. (b) SEM image of a fabricated optic taken at a slightly oblique (10°) angle, illustrating fabrication quality. (c) The simulated phase (red) and transmission (blue) of the unit cell. The widths selected for the pillar library are denoted by red circles. (d) A photograph of the fabricated optics. A person is holding the compensator optic in the foreground while the variator (left) and focusing (right) optics are resting on the table in the background. (e) A photograph of the meta-optics in the experiment setup.

The imaging quality of the meta-optical system was characterized in a simple experimental setup consisting of an illumination source and target object, a narrowband filter, the meta-optics, relay optics, and a camera sensor. A photograph of the fabricated optics in the measurement setup is shown in Fig. 2(e). As the source of MWIR illumination, we use a hot plate (Torrey Pines Scientific HP50) set to 130 °C. This provides broadband infrared radiation that we filter to a narrower band near the design wavelength using a narrowband filter (Thorlabs FB3500-500, with 3.5 μm center wavelength and FWHM bandwidth of 500 nm). A matte black anodized aluminum target projecting the USAF 1951 resolution chart is placed just after the hot plate to form the imaging object. In order to demonstrate imaging up to 50° FoV, we place the target at a distance D from the first meta-optic such that the edges of the target are 25° from normal incidence. For our target, which is 12.5 cm wide, this corresponds to $D = 13.4$ cm in imaging experiments. Images were collected on a FLIR A6751 MWIR InSb camera sensor with 640×512 pixels at 15 μm per pixel resolution. Due to the camera sensor being located further than the designated 15 mm back focal length inside the protective camera housing, it was necessary to use relay optics to re-image the meta-optics image onto the sensor. For this purpose, we used an F/1 MWIR-coated, germanium plano-convex singlet lens (Edmund Optics #69-649, 25 mm focal length) with an F/2.5 compound refractive lens assembly (FLIR #4218538, 25 mm focal length). To ensure that the relay optics do not restrict measurement of the meta-optics, we ensure that the numerical aperture (NA) of the relay optics ($NA > 0.45$) exceeds the maximum NA of the meta-optic zoom system ($NA = 0.42$). The relay optics additionally aid in the precise alignment of the system; details of the alignment procedure are provided in the [supplementary material](#).

The simulated and experimental imaging results for all five configurations are shown in Fig. 3, with the USAF resolution target positioned such that the horizontal edges of the imaging target correspond

to a 50° full FoV. To correct for noise due to ambient radiation on the sensor, we performed a flat field correction on all experimental results by collecting an image with the object blocked and subtracting that background image from the signal; the resulting image captures are shown in Fig. 3(a). We observe good imaging quality and close agreement with the simulated results shown in Fig. 3(c). However, the somewhat broad linewidth of the illumination source (approximately 500 nm FWHM with the narrowband filter) introduces chromatic aberrations that reduce the sharpness of the image as compared to a single-wavelength measurement. To mitigate this effect, simple computational postprocessing techniques can be introduced to improve the image quality. In Fig. 3(b), we show the experiment imaging results after postprocessing with a Gaussian kernel sharpening filter and bm3d denoising algorithm.²⁷ While there still exists some diffuse noise that we attribute primarily to reflections from the narrowband filter, the USAF groups are effectively sharpened for close qualitative agreement with the simulated single-wavelength results in Fig. 3(c). Moving from left to right, the system exhibits clear zoom functionality and qualitatively good imaging performance in configurations 1–5, as well as close agreement between the simulation and experiment.

While this zoom lens system was optimized for single-wavelength illumination at 3.4 μm , we demonstrate high-quality imaging over a wavelength band of approximately 500 nm. In meta-optics (and other forms of diffractive optics) with set phase wraps, the focal length is inversely proportional to the optical wavelength.²⁸ Therefore, the light of different wavelengths does not focus in the same plane, leading to chromatic aberrations. Despite this effect, we demonstrate relatively good imaging quality with the addition of a narrowband filter. While single-wavelength rather than broadband illumination is predicted to improve imaging performance in simulation, further filtering ambient light to a narrower range would also reduce the signal to noise ratio (SNR) due to the reduced light entering the system,

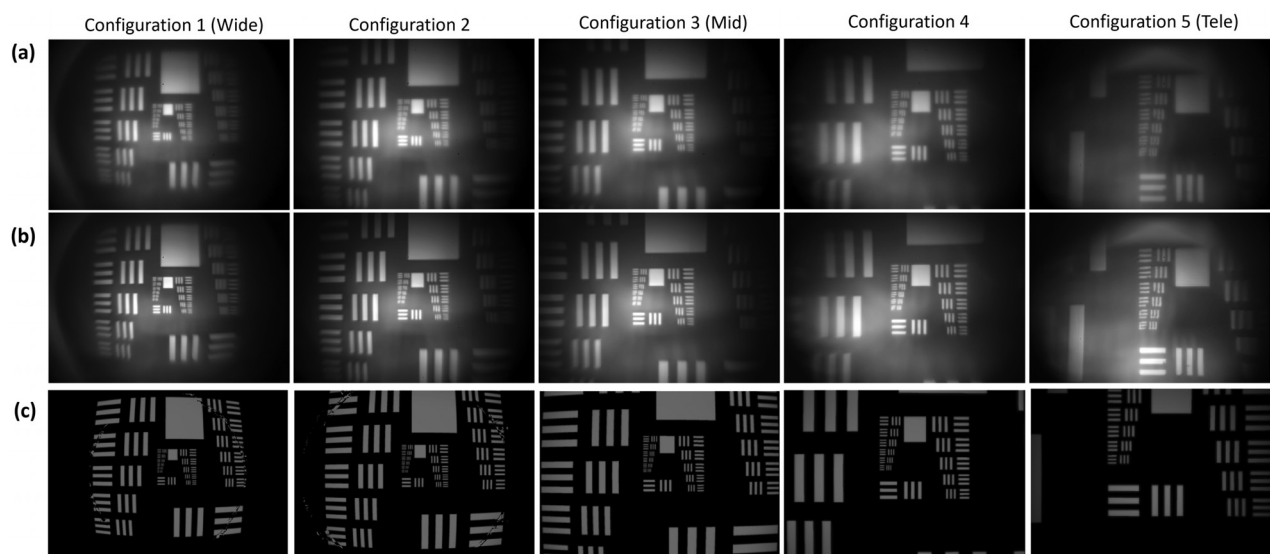


FIG. 3. Simulated and experimental imaging results. (a) Experiment imaging results for configurations 1 (left) through 5 (right). The imaging object, a hot plate and USAF resolution chart, is placed such that the edges of the target cover 50° FoV with respect to the meta-optics. (b) Experimental results that have been computationally enhanced with sharpening and denoising. (c) Simulated imaging results via ray tracing.

unless some active illumination source (such as an LED or laser) is used to illuminate the target. However, such active illumination would be impractical for many applications of this zoom system, such as remote sensing. Therefore, we present imaging results over a broader band, for higher SNR, coupled with computational postprocessing to regain some quality lost due to undesirable chromatic effects. Extension to broader bandwidth operation may be possible using dispersion engineering²⁹ to match the required phases over a range of wavelengths or applying inverse design techniques³⁰ to extend the operating wavelength range.

In multi-element optical systems such as this one, misalignment can have deleterious effects on lens performance. To quantify the effects of misalignment on the performance of the system, we performed a simulated tolerance analysis of configuration 1 in Zemax at the design wavelength of $3.4\ \mu\text{m}$, shown in Fig. 4. The nominal MTF is shown in Fig. 4(a). In the absence of misalignment, the imaging performance is nearly diffraction limited at normal incidence and decreases slightly at larger angles of incidence. As a metric of lens system performance, we report the average (sagittal and tangential) MTF at 20 lp/mm resolution as a function of alignment tolerances. As illustrated in Fig. 4(b), we specifically consider the effects of translation in Z (axial displacement), translation in X/Y (decentering), and rotation about the X axis (tilt). We varied each category of misalignment separately in this analysis. In detail, we conducted a Monte Carlo analysis comprising 20 trials wherein each element was misaligned by a random amount within the specified tolerance along the horizontal axis. We considered reasonable experimental alignment tolerances of up to 1 mm of translation and

up to 5° of tilt in each element. In Figs. 4(c)–4(e), we report the average MTF value as a function of worsening misalignment for angles of incidence up to 25° . As expected, the average MTF decreases with increasing misalignment; however, this decrease is approximately linear. This indicates robustness in the system that we attribute to the relatively small phase gradient of each metasurface.

At MWIR wavelengths in particular, silicon-based meta-optics are a promising alternative to expensive and limited MWIR refractive lens materials like germanium and calcium fluoride. Our choice of silicon-on-sapphire platform, as opposed to all-silicon, was motivated by the presence of significant undesirable reflections in an all-silicon substrate. However, anti-reflective coatings, such as a layer of ZnS,^{25,31} have been shown to improve transmission at infrared wavelengths. The design approach demonstrated here is agnostic to the material platform and could likely be adapted to other MWIR meta-optic materials, such as silicon.^{32,33}

Our meta-optics-based zoom lens system achieves a zoom range of $5\times$, which is sufficient for many applications. To further increase the zoom range, it would generally require decreasing the NA of the system, which results in reduced imaging quality and field of view.⁶ Similarly to refractive optics, additional layers of optics provide degrees of freedom that can be used to improve performance and achieve additional functionalities, such as increased zoom range. This demonstration of a meta-optic triplet system highlights the potential for meta-optics to replace refractive elements in increasingly complex multi-layer and multi-functional imaging systems. In particular, we envision meta-optical systems like this one finding utility in weight-

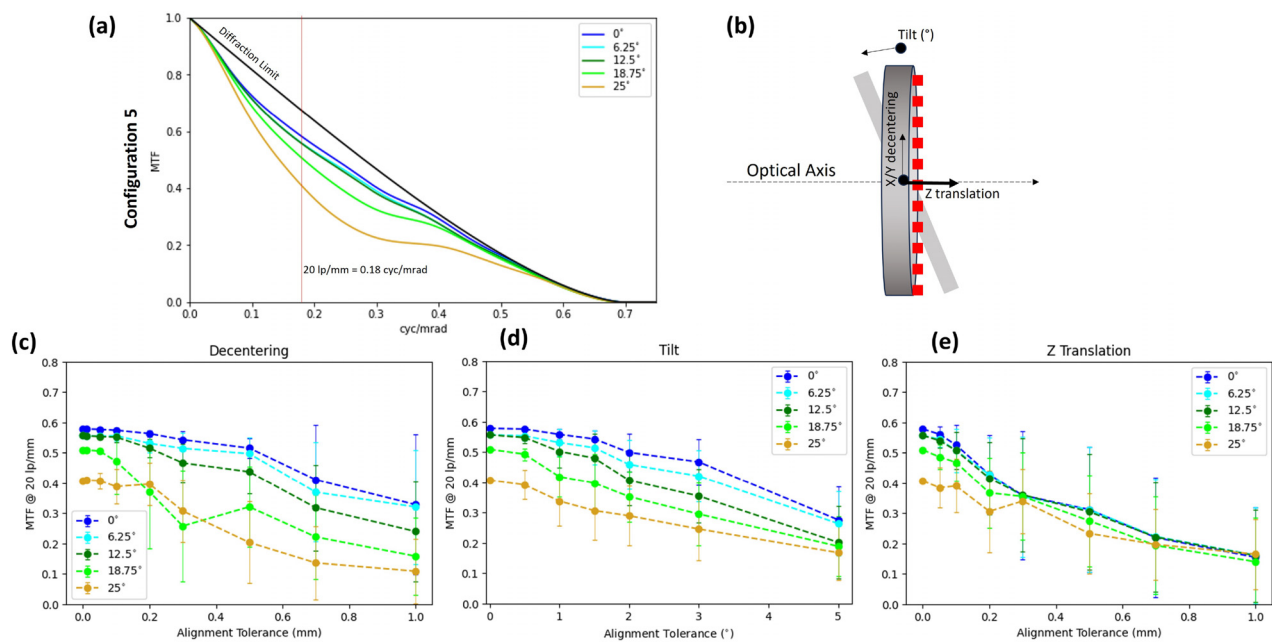


FIG. 4. Simulated tolerance to meta-optic misalignment. (a) Nominal MTF for configuration 1 for angles of incidence up to 25° . The reported MTF is the average over both sagittal and tangential directions. The diffraction limit is plotted in black for comparison. The vertical red line indicates the $20\ \text{lp/mm} = 0.18\ \text{cyc/mrad}$ resolution that was chosen as a metric for the tolerance analysis. (b) Schematic depicting the categories of misalignments that were considered. In the Monte Carlo analysis, all three metasurfaces were misaligned according to the specified tolerances. (c)–(e) Tolerance analysis for the wide configuration. For each field (up to 25°), we plot the MTF at 20 lp/mm as a function of allowed misalignment. The misalignment is decentering in (c), tilt in (d), and axial translation in (e). The error bars represent one standard deviation from Monte Carlo analysis consisting of 20 trials.

constrained systems requiring zoom functionality and a wide field of view, such as airborne remote sensing applications.

See the [supplementary material](#), which includes a table of the optimized metasurface phase coefficients and a written description of the optical alignment procedure.

Part of this work was conducted at the Washington Nanofabrication Facility/Molecular Analysis Facility, a National Nanotechnology Coordinated Infrastructure (NNCI) site at the University of Washington with partial support from the National Science Foundation via Award Nos. NNCI-1542101 and NNCI-2025489.

Funding for this work was supported by the federal STTR program.

AUTHOR DECLARATIONS

Conflict of Interest

Yes, A.M. is a co-founder of Tunoptix, which is commercializing similar meta-optics in the visible. Z.C. and A.M.J. work at CFDR, which is commercializing infrared imaging systems.

Author Contributions

Anna Wirth-Singh: Data curation (lead); Investigation (lead); Writing – original draft (lead). **Arturo Martin Jimenez:** Conceptualization (equal); Formal analysis (equal); Investigation (equal). **Minho Choi:** Investigation (supporting); Methodology (supporting); Writing – review & editing (supporting). **Johannes E. Fröch:** Supervision (supporting); Writing – review & editing (supporting). **Rose Johnson:** Investigation (supporting); Writing – review & editing (supporting). **Tina Le Teichmann:** Investigation (supporting). **Zachary Coppens:** Conceptualization (equal); Funding acquisition (equal); Supervision (supporting). **Arka Majumdar:** Conceptualization (equal); Funding acquisition (equal); Project administration (equal); Supervision (lead).

DATA AVAILABILITY

The data that support the findings of this study are available from the corresponding authors upon reasonable request.

REFERENCES

- X. Wei, L. Xu, J. Zhao, and S. Geng, “Optical design of a continuous zoom MWIR lens system with large field of view,” *Proc. SPIE* **12935**, 1293505 (2023).
- M. C. Sanson and J. Cornell, “MWIR continuous zoom with large zoom range,” *Proc. SPIE* **7660**, 77601X (2010).
- A. N. Wilson, K. A. Gupta, B. H. Koduru, A. Kumar, A. Jha, and L. R. Cenkeramaddi, “Recent advances in thermal imaging and its applications using machine learning: A review,” *IEEE Sens. J.* **23**, 3395–3407 (2023).
- J. P. Estrera, T. E. Ostromek, W. Isbell, and A. V. Bacarella, “Modern night vision goggles for advanced infantry applications,” *Proc. SPIE* **5079**, 486380 (2003).
- V. Dhar and Z. Khan, “Comparison of modeled atmosphere-dependent range performance of long-wave and mid-wave ir imagers,” *Infrared Phys. Technol.* **51**, 520–527 (2008).
- J. Zhang, Q. Sun, Z. Wang, G. Zhang, Y. Liu, J. Liu, E. R. Martins, T. F. Krauss, H. Laign, J. Li, and X.-H. Wang, “A fully metaoptical zoom lens with a wide range,” *Nano Lett.* **24**, 4893–4899 (2024).
- M. Y. Shalaginov, S. An, F. Yang, P. Su, D. Lyzwa, A. M. Agarwal, H. Zhang, J. Hu, and T. Gu, “Single-element diffraction-limited fisheye metalens,” *Nano Lett.* **20**, 7429–7437 (2020).

- S. Yue, Y. Liu, R. Wang, Y. Hou, H. Shi, Y. Feng, Z. Wen, and Z. Zhang, “All-silicon polarization-independent broadband achromatic metalens designed for the mid-wave and long-wave infrared,” *Opt. Express* **31**, 44340–44352 (2023).
- K.-H. Shih and C. K. Renshaw, “Broadband metasurface aberration correctors for hybrid meta/refractive mwir lenses,” *Opt. Express* **30**, 28438–28453 (2022).
- S. So, J. Mun, J. Park, and J. Rho, “Revisiting the design strategies for metasurfaces: Fundamental physics, optimization, and beyond,” *Adv. Mater.* **35**, 2206399 (2023).
- M. Choi, J. Park, J. Shin, H. Keawmuang, H. Kim, J. Yun, J. Seong, and J. Rho, “Realization of high-performance optical metasurfaces over a large area: A review from a design perspective,” *npj Nanophotonics* **1**, 31 (2024).
- H.-S. Ee and R. Agarwal, “Tunable metasurface and flat optical zoom lens on a stretchable substrate,” *Nano Lett.* **16**, 2818–2823 (2016).
- S. M. Kamali, E. Arbabi, A. A. Y. Horie, and A. Faraon, “Highly tunable elastic dielectric metasurface lenses,” *Laser Photonics Rev.* **10**, 1002–1008 (2016).
- A. She, S. Zhang, S. Shian, D. R. Clarke, and F. Capasso, “Adaptive metalenses with simultaneous control of focal length, astigmatism, and shift,” *Sci. Adv.* **4**, eaap9957 (2018).
- E. Arbabi, A. Arbabi, S. M. Kamali, Y. Horie, M. Faraji-Dana, and A. Faraon, “MEMS-tunable dielectric metasurface lens,” *Nat. Commun.* **9**, 812 (2018).
- C. Jung, E. Lee, and J. Rho, “The rise of electrically tunable metasurfaces,” *Sci. Adv.* **10**, eado8964 (2024).
- M. Bosch, M. R. Shcherbakov, K. Won, H.-S. Lee, Y. Kim, and G. Shvets, “Electrically actuated varifocal lens based on liquid-crystal-embedded dielectric metasurfaces,” *Nano Lett.* **21**, 3849 (2021).
- A. Zhan, S. Colburn, C. M. Dodson, and A. Majumdar, “Metasurface freeform nanophotonics,” *Sci. Rep.* **7**, 1673 (2017).
- S. Colburn, A. Zhan, and A. Majumdar, “Varifocal zoom imaging with large area focal length adjustable metalenses,” *Optica* **5**, 825 (2018).
- A. Arbabi, E. Arbabi, S. M. Kamali, Y. Horie, S. Han, and A. Faraon, “Miniature optical planar camera based on a wide-angle metasurface doublet corrected for monochromatic aberrations,” *Nat. Commun.* **7**, 13682 (2016).
- B. Groever, W. T. Chen, and F. Capasso, “Meta-lens doublet in the visible region,” *Nano Lett.* **17**, 4902–4907 (2017).
- Y. Park, B. Lee, and Y. Jeong, “End-to-end optimization of meta-lens doublet for high-quality wide-angle imaging,” *Proc. SPIE* **12646**, 126460D (2023).
- S. Shrestha, A. Overvig, M. Lu, A. Stein, and N. Yu, “Multi-element metasurface system for imaging in the near-infrared,” *Appl. Phys. Lett.* **122**, 2001701 (2023).
- C.-F. Pan, H. Wang, H. Wang, P. N. S. adn Qifeng Ruan, S. Wredh, Y. Ke, J. Y. E. Chan, W. Zhang, C.-W. Qiu, and J. K. Yang, “3D-printed multilayer structures for high-numerical aperture achromatic metalenses,” *Sci. Adv.* **9**, eadj9262 (2023).
- J. T. Cox and G. Hass, “Antireflection coatings for germanium and silicon in the infrared,” *J. Opt. Soc. Am.* **48**, 677–680 (1958).
- V. Liu and S. Fan, “S4: A free electromagnetic solver for layered periodic structures,” *Comput. Phys. Commun.* **183**, 2233–2244 (2012).
- Y. Mäkinen, L. Azzari, and A. Foi, “Collaborative filtering of correlated noise: Exact transform-domain variance for improved shrinkage and patch matching,” *IEEE Trans. Image Process.* **29**, 8339–8354 (2020).
- L. Huang, S. Colburn, A. Zhan, and A. Majumdar, “Full-color metaoptical imaging in visible light,” *Adv. Photonics Res.* **3**, 2100265 (2022).
- W. T. Chen, A. Y. Zhu, and F. Capasso, “Flat optics with dispersion-engineered metasurfaces,” *Nat. Rev. Mater.* **5**, 604–620 (2020).
- L. Huang, Z. Han, A. Wirth-Singh, V. Saragadam, S. Mukherjee, J. E. Fröch, Q. A. A. Tanguy, J. Rollag, R. Gibson, J. R. Hendrickson, P. W. C. Hon, O. Kigner, Z. Coppens, K. F. Böhringer, A. Veeraraghavan, and A. Majumdar, “Broadband thermal imaging using meta-optics,” *Nat. Commun.* **15**, (2024).
- H. C. Nalbant, F. Balli, T. Yelboga, A. Eren, and A. Sozak, “Transmission optimized lwir metalens,” *Appl. Opt.* **61**, 9946 (2022).
- Y. Yang, H. Kang, C. Jung, J. Seong, N. Jeon, J. Kim, D. K. Oh, J. Park, K. Kim, and J. Rho, “Revisiting optical material platforms for efficient linear and non-linear dielectric metasurfaces in the ultraviolet, visible, and infrared,” *ACS Photonics* **10**, 307 (2023).
- L. Huang, Z. Coppens, K. Hallman, Z. Han, K. F. Böhringer, N. Akozbek, A. Raman, and A. Majumdar, “Long wavelength infrared imaging under ambient thermal radiation via an all-silicon metalens,” *Opt. Mater. Express* **11**, 2907 (2021).